Proc. Natl. Acad. Sci. USA
Vol. 88, pp. 3479–3483, April 1991
Biochemistry

Secondary structure of the phosphocarrier protein III^{Glc}, a signal-transducing protein from *Escherichia coli*, determined by heteronuclear three-dimensional NMR spectroscopy

(phospho*enol*pyruvate:glycose phosphotransferase system/phosphohistidine/triple resonance)

JEFFREY G. PELTON*, DENNIS A. TORCHIA*, NORMAN D. MEADOW†, CING-YUEN WONG†, AND SAUL ROSEMAN†

*Bone Research Branch, National Institute of Dental Research, National Institutes of Health, Bethesda, MD 20892; and †Department of Biology and McCollum-Pratt Institute, The Johns Hopkins University, Baltimore, MD 21218

Contributed by Saul Roseman, December 19, 1990

ABSTRACT **III^{Glc} is a signal-transducing phosphocarrier protein of the phospho*enol*pyruvate:glycose phosphotransferase system of *Escherichia coli*. The secondary structure of III^{Glc} is determined by heteronuclear (^{15}N, ^{13}C) three-dimensional NMR spectroscopy. Sequential, medium-range, and long-range nuclear Overhauser effects seen in NMR spectra are used to elucidate 11 antiparallel β-strands and four helical segments. The medium-range nuclear Overhauser effect patterns suggest that the helices are either distorted α-helices or are of the 3_{10} class. The amino acids separating the active-site histidine residues (His^{75} and His^{90}) form two strands (Ala^{76}-Ser^{81} and Val^{85}-Phe^{91}) of a six-stranded antiparallel β-sheet that brings His^{90} and His^{75} in close proximity. Sequence similarities in III^{Glc} and several other sugar-transport proteins suggest that the histidine residues within these proteins may be arranged in a similar manner. The 18-residue N-terminal peptide that precedes β-strand Thr^{19}-Ile^{22} in native III^{Glc} is disordered and does not interact with the rest of the protein. Furthermore, removal of the N-terminal heptapeptide by a specific endopeptidase does not affect the structure of the remaining protein, thus explaining the phospho-acceptor activity of modified III^{Glc} with the phospho-histidine-containing phosphocarrier protein of this system.**

The bacterial phospho*enol*pyruvate:glycose phosphotransferase system (PTS) was first recognized as a sugar phosphorylating/transport system and subsequently as a key regulatory system for other processes. Many of the latter functions, such as diauxic growth, involve transduction of signals from the environment to the genome, thereby initiating or repressing the transcription of certain operons. The *crr* gene was found to be essential for these regulatory processes, and this gene was shown to encode the PTS phosphocarrier protein, III^{Glc} (18.1 kDa). III^{Glc} fulfills its many functions by interacting with membrane-bound and cytoplasmic proteins including the PTS proteins phosphohistidine-containing phosphocarrier protein of the PTS (HPr), enzyme II^{Glc}, enzyme IIB^{Bgl}, and the non-PTS proteins adenylate cyclase, glycerol kinase, and the melibiose, lactose, and maltose permeases (for recent reviews, see refs. 1–3).

Biochemical and physical methods have revealed several regions of III^{Glc} important for activity. HPr phosphorylates His^{90} at the N-3 position (4), and replacement of this histidine residue with glutamine completely inactivates the protein. In contrast, replacement of His^{75} with glutamine results in the loss of phospho-donor but not phospho-acceptor activity, indicating that both histidine residues are required for normal function (5). Furthermore, cleavage of the N-terminal heptapeptide by a membrane-associated endopeptidase reduces phospho-donor activity by 97% (6), whereas derivitization of Gly^1 reduces this activity 80% (7). These results suggest that the N terminus is important in formation of the binary III^{Glc}–II^{Glc} complex.

Early NMR investigations of PTS proteins centered around HPr (8, 9), factor III from the lactose PTS (III^{Lac}) (10), and III^{Glc} (4). To date, however, the detailed structure of only one protein of this system, HPr, has been determined by NMR (11–13) and x-ray crystallographic (14) methods.

We have completed (98%) assignment of the backbone ^{15}N, ^{13}C, and ^1H resonances of III^{Glc} (168 amino acids) with a battery of three-dimensional (3D) triple-resonance NMR experiments (15, 16) and have assigned the side-chain ^1H and ^{13}C resonances by using 3D ^1H-^{13}C-^{13}C-^1H-correlation spectroscopy (HCCH–COSY) (17, 18) and ^1H-^{13}C-^{13}C-^1H-total correlation spectroscopy (HCCH–TOCSY) (19) spectra (J.G.P. and D.A.T., unpublished results). These experiments, which rely on single-bond J couplings, yield assignments without reference to secondary structure, in contrast to standard methods using correlation spectroscopy (COSY) and nuclear Overhauser effect spectroscopy (NOESY) spectra (20–22). The assignments enable us to analyze 3D ^{15}N and ^{13}C NOESY–heteronuclear multiple quantum spectroscopy (HMQC) spectra (23–25) of III^{Glc} and elucidate its secondary structure in a manner similar to that used for interleukin 1β (26). Herein we present detailed information on the secondary structure of III^{Glc} and correlate the results with information about function derived from biochemical studies.

MATERIALS AND METHODS

Growth of Bacteria and Purification of III^{Glc}. The coding sequence of the *crr* gene was cloned into the *Nde* I–*Eco*RI sites of pVEX-11 (a gift from V. Chaudhary, Laboratory of Molecular Biology, National Institutes of Health) under control of the T7 promotor. *Escherichia coli* strain BL21 (DE3) (27) was transformed with plasmid pVEX-crr and grown in the minimal medium of Neidhardt *et al.* (28) with 0.2% glucose used as carbon source (see below) and supplemented with thiamine at 2 μg/ml and ampicillin at 50 μg/ml.

The publication costs of this article were defrayed in part by page charge payment. This article must therefore be hereby marked "*advertisement*" in accordance with 18 U.S.C. §1734 solely to indicate this fact.

Abbreviations: NOE, nuclear Overhauser effect; NOESY, nuclear Overhauser effect spectroscopy; NOESY–HMQC, NOE–heteronuclear multiple quantum spectroscopy; COSY, correlation spectroscopy; HCCH–COSY, ^1H-^{13}C-^{13}C-^1H correlation spectroscopy; HCCH–TOCSY, ^1H-^{13}C-^{13}C-^1H–total correlation spectroscopy; DANTE, delays alternating with nutation for tailored excitation; PTS, phospho*enol*pyruvate:glycose phosphotransferase system; 3D, three-dimensional; III^{Glc}, phosphocarrier protein of the PTS of *Escherichia coli*; HPr, histidine-containing phosphocarrier protein of the PTS.

[^{15}N]Ammonium chloride or [^{15}N]ammonium chloride/[^{13}C]-glucose (MSD Isotopes) were used as the sole nitrogen source or as sole nitrogen/carbon sources, respectively. When cultures reached an absorbance of 2–2.5 at 500 nm, isopropyl β-D-thiogalactoside was added (1 mM), to induce synthesis of III^{Glc}. After 2 hr of further growth, cells were harvested.

The cells were disrupted in a French pressure cell; streptomycin sulfate was added (1.3%), and the homogenate was centrifuged at 200,000 × *g* for 1 hr. III^{Glc} in the supernatant was purified by a modification of procedure A (29) that will be described in detail elsewhere. The procedure yielded 25 mg of III^{Glc} per 3 g of cell paste per liter of medium. III^{Glc} was >97% pure, as determined by SDS/PAGE and then quantitative densitometric scanning of the Coomassie-stained gel. Amide protons were exchanged for deuterons by dissolving a sample in ^2H_2O, heating overnight at 42°C, and reheating at 48°C for 18 hr. The final ^{15}N- and ^{15}N/^{13}C-enriched samples consisted of 1.6 mM III^{Glc} and 0.15 M KCl (pH 6.4, uncorrected for isotope effects) in 90% H_2O/10% ^2H_2O or 99.996% ^2H_2O (Cambridge Isotope Laboratories, Woburn, MA), respectively.

NOESY. 3D NOESY–HMQC spectra were obtained on a modified AM-500 spectrometer (16). The 3D ^{15}N NOESY–HMQC pulse sequence used was the same as that described (23, 24), except that the ^{1}H 1:1 water-suppression pulse was replaced with a hard ^{1}H 90° pulse, and presaturation was accomplished by a 30-Hz off-resonance DANTE (delays alternating with nutation for tailored excitation) pulse (24). ^{1}H and ^{15}N channels were set to 8.67 ppm and 118.5 ppm, respectively, with spectral widths of 5000 Hz (t_1), 2000 Hz (t_2), and 4000 Hz (t_3). The 3D ^{13}C NOESY–HMQC pulse sequence was the same as described (25), except that a 180° ^{13}C pulse was used for ^{13}C decoupling in t_1. ^{1}H and ^{13}C channels were set to 4.00 ppm and 43 ppm, respectively, with spectral widths of 4166 Hz (t_1, t_3) and 2994 Hz (t_2). Both spectra were derived from data matrices consisting of 128 (complex) × 32 (complex) × 512 (real) points in t_1, t_2, and t_3, respectively. In addition, in both experiments 64 scans per (t_1, t_2) were signal averaged using a mixing time of 100 ms and a recycle time of 0.9 s at 36.5°C.

Data were transferred to a Sun 4-110 workstation (Sun Microsystems, Milpitas, CA) and processed with a combination of commercial (NMRi, Syracuse, NY) and in-house software (24, 30). Sine-bell and sine-bell-squared window functions were applied in t_1 and t_3, respectively, with phase shifts of 60° (^{15}N) or 45° (^{13}C) in both dimensions. The data were zero-filled once in t_2 and t_3 and twice in t_1, resulting in 512 × 64 × 512 matrices for the absorptive portion of the spectra. Chemical shifts are referenced to H_2O (4.67, 36.5°C), external liquid ammonia (^{15}N), and sodium 3-[2,2,3,3,-$^2H_4$]trimethylsilylpropionate (^{13}C) (31). Uncertainties in chemical shifts are 0.02 ppm and 0.1 ppm for ^{1}H and heteronuclei, respectively.

RESULTS

Identification and sequential assignment of all NH and C$^\alpha$H resonances of III^{Glc}, except for the amide protons of Gly^1, Leu^2, Asn^{57}, Glu^{72}, and Ser^{83} were made through analysis of triple-resonance (^{1}H, ^{13}C, ^{15}N) 3D NMR spectra (15, 16). The assignments were then extended to the C$^\beta$H signals with the exception of Arg^{105} and Met^{148}, as well as to a significant number of other side-chain resonances through analysis of 3D HCCH–COSY (17, 18) and HCCH–TOCSY (19) spectra. In this regard, assignments for residues Asp^4–Ser^8 remain tentative due to limited proteolysis in the N-terminal domain during data acquisition. Previously (27) it was noted that two forms of III^{Glc}, designated III$^{Glc}_{fast}$ and III$^{Glc}_{slow}$, were isolated during purification, and III$^{Glc}_{fast}$ was shown to result from cleavage of the N-terminal heptapeptide of III$^{Glc}_{slow}$ by a membrane-associated endopeptidase (6). We noted that our samples converted from III$^{Glc}_{slow}$ to III$^{Glc}_{fast}$ over several weeks, which was confirmed by nondenaturing PAGE (29) (data not shown). Comparison of ^{15}N and ^{1}H chemical shifts for the two forms revealed no changes, except for residues near the cleavage site, and consequently we could assign all resonances, except for Asp^4-Ser^8. The complete set of spectral assignments will be published elsewhere.

Upon completion of the resonance assignments, we undertook analysis of 3D ^{15}N and ^{13}C NOESY–HMQC spectra (23–25) to gain insight into the structure of III^{Glc}. Cross peak intensities (NOEs) in NOESY spectra acquired with a short mixing time are proportional to the inverse-sixth power of the distance between the spins, and hence, the NOESY spectrum contains information about the spatial arrangement of protons within the molecule. Characteristic patterns of sequential, medium-, and long-range NOEs are used to identify secondary-structural elements of proteins, such as β-pleated sheet and helices (20–22). Ambiguities can arise in the secondary structure determination, however, when attempting to distinguish between helical termini and either tight turns or half turns near the ends of helices because they are characterized by similar sequential and medium-range NOE patterns (20). Therefore, identification of turns is generally postponed and is accomplished during determination of the tertiary structure of the protein.

Portions of 3D ^{15}N and ^{13}C NOESY–HMQC spectra used to obtain short-, medium-, and long-range NOEs are presented in Fig. 1 *A* and *B*, respectively. The regions shown correspond to ^{15}N-^{1}H (Fig. 1*A*) and ^{13}C-^{1}H (Fig. 1*B*) -diagonal and associated cross peaks for residues His^{75}-Ser^{78} and Phe^{88}-Phe^{91}. Fig. 1*A* shows that NOEs are seen between the C$^\alpha$H and at least one C$^\beta$H proton of each residue and its own amide NH, indicating close proximity of these protons, as expected. A complete set of sequential $d_{\alpha N}$ NOEs are also observed for the two segments shown. Strong $d_{\alpha N}$ NOEs indicate that these residues adopt an extended conformation (20). Furthermore, sequential $d_{\beta N}$ NOEs are seen for residues within the two segments, except for His^{90}-Phe^{91}, and finally, a pair of sequential d_{NN} NOEs are observed between His^{75} and Ala^{76}. These NOEs are summarized in Fig. 2. In addition to these short-range connectivities, long-range NOEs are seen in the 3D ^{15}N and ^{13}C NOESY–HMQC spectra (dashed lines, Fig. 1 *A* and *B*). These long-range NOEs are shown graphically in Fig. 3*A*, where it can be seen that the two segments Ala^{76}-Ser^{81} (VI) and Leu^{85}-Phe^{91} (VII), which contain the active-site histidine residues, form a portion of antiparallel β-sheet. Based on this secondary structure, an NOE between the C$^\alpha$H protons of Val^{89} (4.37 ppm) and Val^{138} (4.33 ppm) was expected in the 3D ^{13}C NOESY–HMQC spectrum but is obscured by the intense diagonal peak. An NOE was also expected between Val^{138} C$^\alpha$H and His^{90} NH, but it could not be distinguished from the intraresidue His^{90} C$^\alpha$H-NH NOE due to degeneracy of the Val^{138} (4.33 ppm) and His^{90} (4.33 ppm) C$^\alpha$H protons.

In a similar manner, sequential d_{NN}, $d_{\alpha N}$, $d_{\beta N}$, medium-range $d_{\alpha N}$ (i, i + 2), $d_{\alpha N}$ (i, i + 3), and $d_{\alpha N}$ (i, i + 4), and long-range d_{NN} (i, j) and $d_{\alpha N}$ (i, j) NOEs, where i and j correspond to residues separated by at least five amino acids, were identified in a 3D ^{15}N NOESY–HMQC spectrum. The sequential and medium-range NOEs are summarized in Fig. 2. Inspection of the figure revealed nine other segments that adopt extended conformations and might form β-sheet structures (Fig. 2). The results of a search for long-range NOEs between NH and C$^\alpha$H protons within these segments are summarized in Fig. 3*A*. As can be seen in this figure, III^{Glc} is comprised of an extensive antiparallel β-sheet structure. We note that the chemical shifts of the C$^\alpha$H protons of Glu^{80} (5.12 ppm) and Glu^{86} (5.10 ppm) and the amide protons of Ile^{79}

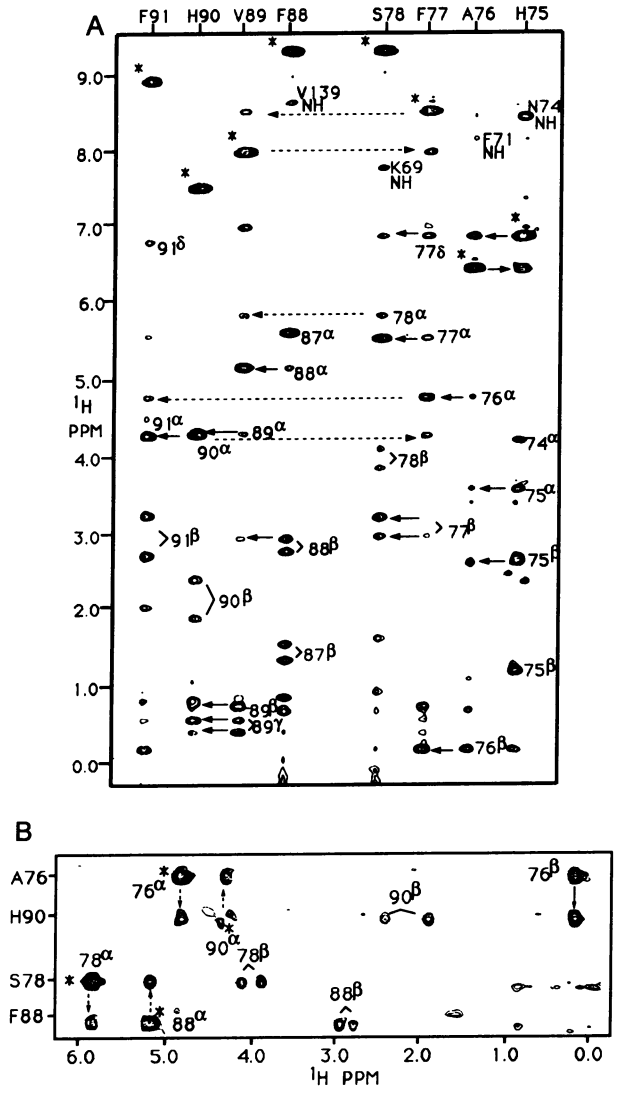

FIG. 1. Composite spectra consisting of strips taken from ^{15}N or ^{13}C planes in 3D ^{15}N (*A*) and ^{13}C (*B*) NOESY–HMQC spectra of III^{Glc} (100-ms mixing time, 36.5°C) showing diagonal and associated cross peaks for segments His^{75}-Ser^{78} and Phe^{88}-Phe^{91}. Asterisks denote ^{15}N-^{1}H and $^{13}C^{\alpha}$-^{1}H diagonal peaks in Fig. 1 *A* and *B*, respectively. Intraresidue $C^{\alpha}H$-NH and $C^{\beta}H$-NH NOEs are denoted with the residue number and either α or β, respectively. Solid arrows, sequential $d_{\alpha N}$, $d_{\beta N}$, and d_{NN} NOEs; dashed arrows, long-range NOEs used to position β-strands VI and VII.

(9.02 ppm) and Leu^{87} (8.99 ppm) are nearly identical. Therefore, the expected β-sheet connectivities $d_{\alpha\alpha}$ (80,86), $d_{\alpha N}$ (80,87), $d_{\alpha N}$ (86,81), and d_{NN} (79,87) could not be clearly identified because they coincided with intense diagonal signals or with strong $d_{\alpha N}$ connectivities. However, the weak NOE between amide protons of Ser^{81} and Leu^{87} and the NOE of moderate intensity between the amide protons of Ser^{81} and Val^{85} show that the β-sheet extends over these residues. Also, the expected NOE between Thr^{136} NH and Lys^{53} $C^{\alpha}H$ (4.70 ppm) could not be observed presumably because this resonance is saturated along with the solvent (4.67 ppm) in the ^{15}N NOESY–HMQC spectrum.

Further inspection of Fig. 2 revealed that the segments Glu^{34}-Gly^{47}, Asp^{94}-Phe^{103}, Pro^{125}-Thr^{134}, denoted HI, HII, and HIII, respectively, can be classified as being in a helical conformation on the basis of strong d_{NN} NOEs and several weaker $d_{\alpha N}$ (i, $i + 2$) and $d_{\alpha N}$ (i, $i + 3$) NOEs (Fig. 1). However, analysis of the 3D ^{13}C NOESY–HMQC spectrum revealed virtually no $d_{\alpha\beta}$ (i, $i + 3$) NOEs. This observation, combined with the presence of a number of $d_{\alpha N}$ (i, $i + 2$) NOEs and a lack of $d_{\alpha N}$ (i, $i + 4$) NOEs, suggests that these helices are either distorted α-helices or are of the 3_{10} class. An interesting feature of segment HI is the break in d_{NN} connectivities between residues Asp^{38} and Val^{39}, which may reflect a disruption of the helix around Pro^{37}. A break in d_{NN} connectivities also occurs at the end of segment HIII between residues Ser^{133} and Thr^{134}, and, in fact, the sequential NOEs of residues Lys^{132}-Leu^{135} taken together are similar to those expected for a half turn or a tight turn of the type II class. As mentioned previously, ambiguities can arise in the resolution of helical termini and turns, precisely because of the similarity of the sequential NOE patterns. Thus, with the presently accumulated data, we are unable to resolve whether these residues are a part of helix HIII or form a turn of one of the types mentioned. The segment Lys^{53}-Gly^{56} and the eight residues after helix HII (Lys^{104}-Ala^{107}, and Glu^{108}-Gln^{111}) also appear, on the basis of sequential and medium-range NOEs, to form either half turns or type II tight turns. Information on the overall fold of the protein is needed to more fully characterize these segments.

Another series of strong sequential d_{NN} NOEs occurs between residues Ser^{141} and Glu^{148} (HIV), indicating that these residues are in a helical conformation. However, the similarity of the $C^{\alpha}H$ protons of Met^{143} (4.43 ppm), Asp^{144} (4.48 ppm), Glu^{145} (4.44 ppm), Ile^{146} (4.42 ppm), and Lys^{147} (4.48 ppm) precluded identification of medium-range $d_{\alpha N}$ (i, $i + 2$) and $d_{\alpha N}$ (i, $i + 3$) NOEs. Moreover, no $d_{\alpha\beta}$ (i, $i + 3$) NOEs were observed, suggesting that helix IV is also a distorted α-helix or of the 3_{10} class.

Not shown in Fig. 3*A* is an extended segment (Ser^{153}-Val^{163}) that connects β-strands X and XI. The sequential NOEs for this region indicate a number of residues in an extended conformation (Val^{156}-Thr^{161}) followed by two segments separated by Pro^{162} with helical/turn character (Gly^{159}-Thr^{161}, Val^{163}-Ile^{164}). In addition to the sequential NOEs, a number of long-range NOEs have been identified between this segment and residues Ile^{23}-Val^{31}. In particular, NOEs are observed in the 3D ^{15}N NOESY–HMQC spectrum between Ile^{23} NH and both Pro^{162} $C^{\alpha}H$ and Val^{163} NH, and between amide protons of the pairs Gly^{28}-Val^{156}, Ile^{30}-Gly^{154}, and Val^{31}-Lys^{151}. Furthermore, an NOE has been identified in the 3D ^{13}C NOESY–HMQC spectrum between $C^{\alpha}H$ protons of Ile^{23} and Pro^{162}, which, together with the ^{15}N data, indicates the close proximity of these segments.

Long-range NOEs that are indicative of tertiary contacts have also been identified in two other regions of the protein. The first set connects the segment Met^{59}-Val^{61}, which has an extended conformation, to the segment Val^{115}-Ile^{120}, which shows a high degree of helical or turn character (Fig. 3*B*). The second set of long-range NOEs connects the C-terminal region of segment HII to the N-terminal region of HIII. Specifically, NOEs are observed between Asp^{123} NH and Gly^{102} $C^{\alpha}H$ and the $C^{\alpha}H$ protons of Phe^{103} and Phe^{122}.

Finally, the first 18 amino acids (Gly^{1}-Gly^{18}) deserve mention. These residues are characterized by relatively few sequential or long-range NOEs (Fig. 2). In addition, these residues show particularly strong cross peaks and narrow line widths in ^{13}C-^{1}H HCCH–COSY and HCCH–TOCSY spectra (data not shown), which are indicative of nuclei that have large spin–spin relaxation times (T_2s). Furthermore, cleavage of the first 7 amino acids by an endopeptidase (6) had no effect on the ^{15}N or ^{1}H chemical shifts (spectra not shown) of the other residues, except near the cleavage site, indicating the structure of the protein remained intact. Thus, on the basis of these data, we conclude that the first 18 amino acids are highly flexible and do not interact significantly with the rest of the protein.

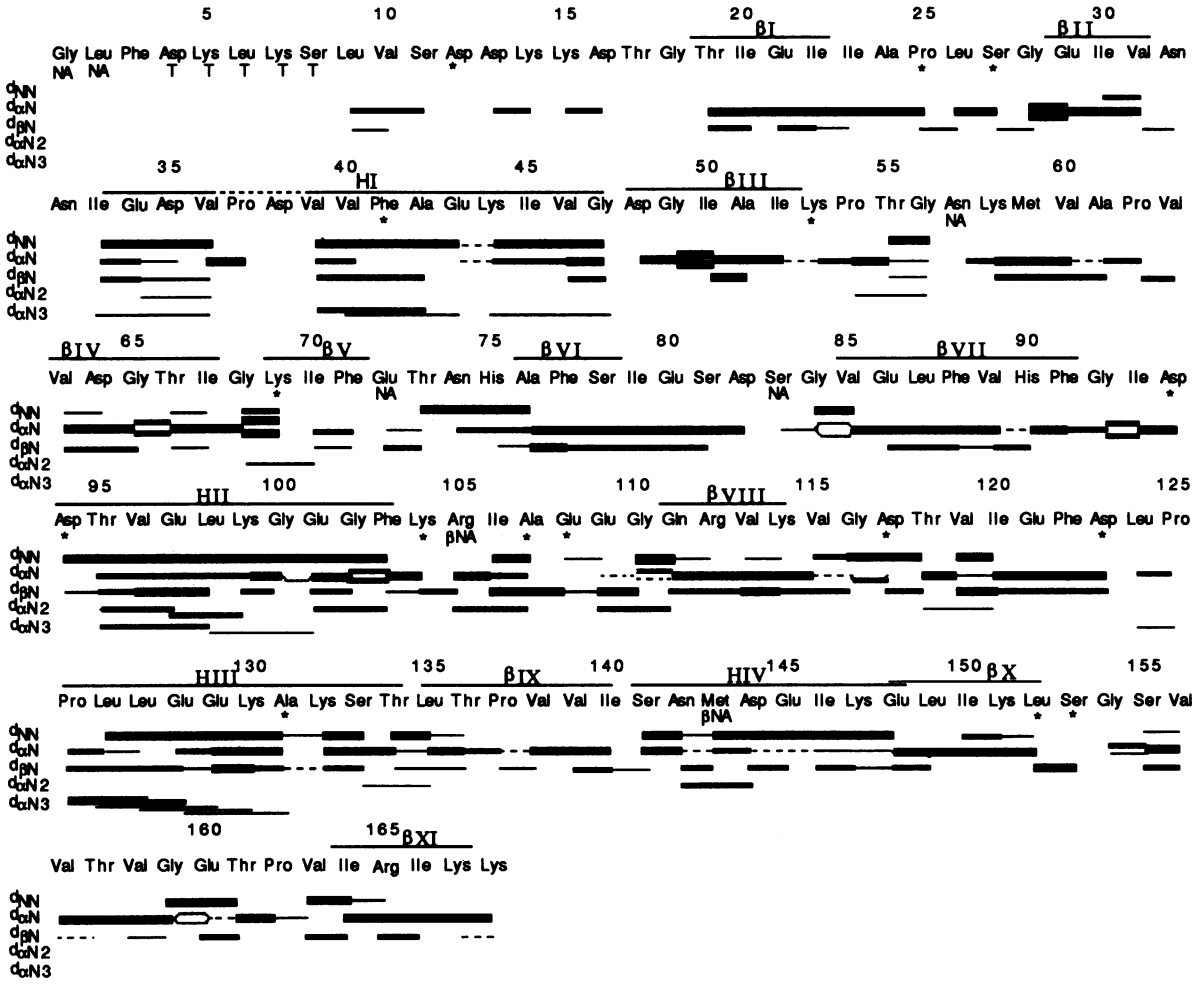

FIG. 2. Summary of sequential and medium-range NOEs observed in a ^{15}N NOESY–HMQC experiment with a mixing time of 100 ms (36.5°C). Medium-range $d_{\alpha N}(i, i + 2)$ and $d_{\alpha N}(i, i + 3)$ NOEs are denoted $d_{\alpha N2}$ and $d_{\alpha N3}$, respectively. Proline $d_{\alpha\delta}(i, i + 1)$ and/or $d_{N\delta}(i, i + 1)$ NOEs observed in 3D ^{13}C and ^{15}N NOESY–HMQC spectra are indicated as $d_{\alpha N}$ connectivities. Cross peaks were classified as strong, medium, or weak; line thickness is used to represent cross-peak intensity. Dashed lines indicate overlap of two or more resonances. H and β denote those residues in helical regions and β-strands, respectively. The helical regions may be slightly shorter than represented due to ambiguities in differentiation of helical termini and turns (see text). Asterisks under amino acid labels denote $C^{\alpha}H$ protons that resonate near H_2O (4.67 ± 0.05 ppm) and, as a consequence, were at least partially saturated by the off-resonance DANTE presaturation pulse. T, residue is tentatively assigned; NA and βNA, amide NH or $C^{\beta}H$ protons, respectively, were not assigned. Note that Asn^{32}, Val^{63}, Asp^{94}, Pro^{125}, and Val^{156} have been repeated on each side of figure.

DISCUSSION

The pattern of sequential and long-range NOEs observed in 3D ^{15}N and ^{13}C NOESY–HMQC spectra shows that III^{Glc} contains extensive antiparallel β-sheet structure, 11 segments in all (Figs. 2 and 3). The presence of strong sequential d_{NN} and medium-range $d_{\alpha N}(i, i + 2)$ and $d_{\alpha N}(i, i + 3)$ NOEs shows, in addition, that four helical segments exist. The observation of a number of $d_{\alpha N}(i, i + 2)$ NOEs together with the absence of $d_{\alpha\beta}(i, i + 3)$ and $d_{\alpha N}(i, i + 4)$ NOEs suggest that these helices are either distorted α-helices or are of the 3_{10} type. Helices of the 3_{10} type have recently been shown to be more common in proteins that have a high proportion of β structure (32).

His^{90}, the target of phospho-HPr (4), resides near the C terminus of β-strand VII. Furthermore, His^{75}, which is necessary for phospho-donor activity (5), resides in a loop at the N terminus of strand VI and is in close proximity to His^{90}. The fact that these residues are close in space lends support to the possibility that phosphate transfer to sugar occurs via phosphate migration between the two histidines (5). Moreover, these histidine residues, along with a majority of the intervening amino acids, are part of a conserved sequence found near the C terminus of five transport proteins found in both Gram-negative and Gram-positive bacteria (1, 33), and therefore the observed secondary structure of this segment from III^{Glc} from *E. coli* may be common to the other proteins as well.

An interesting feature of the β-sheet just discussed is that it is composed of residues in the C-terminal segment (XI) and the residues in the N-terminal segment (I) that exhibit secondary structure. The 18 residues on the N-terminal side of segment I are highly flexible and show no evidence of structure. Moreover, the equality of ^{15}N and ^{1}H chemical shifts of the intact and N-terminal cleaved proteins shows that the N terminus of III^{Glc} does not interact significantly with the remainder of the protein. These conclusions appear to be at odds with the observation that modification of the N terminus by either cleavage of the first seven residues (6) or by derivitization of Gly^{1} (7) results in a pronounced decrease in phospho-donor activity. However, III^{Glc} functions as a phospho-donor at the cell membrane; therefore, we propose that the N-terminal residues of III^{Glc} adopt a more ordered structure upon interaction with components of the cell membrane.

It has been found that the cleaved form of III^{Glc}_{fast} crystallizes much more readily than the intact form (III^{Glc}_{slow}) (D. Worthylake, S. J. Remington, Univ. of Oregon, personal communication). This result is consistent with our observation that

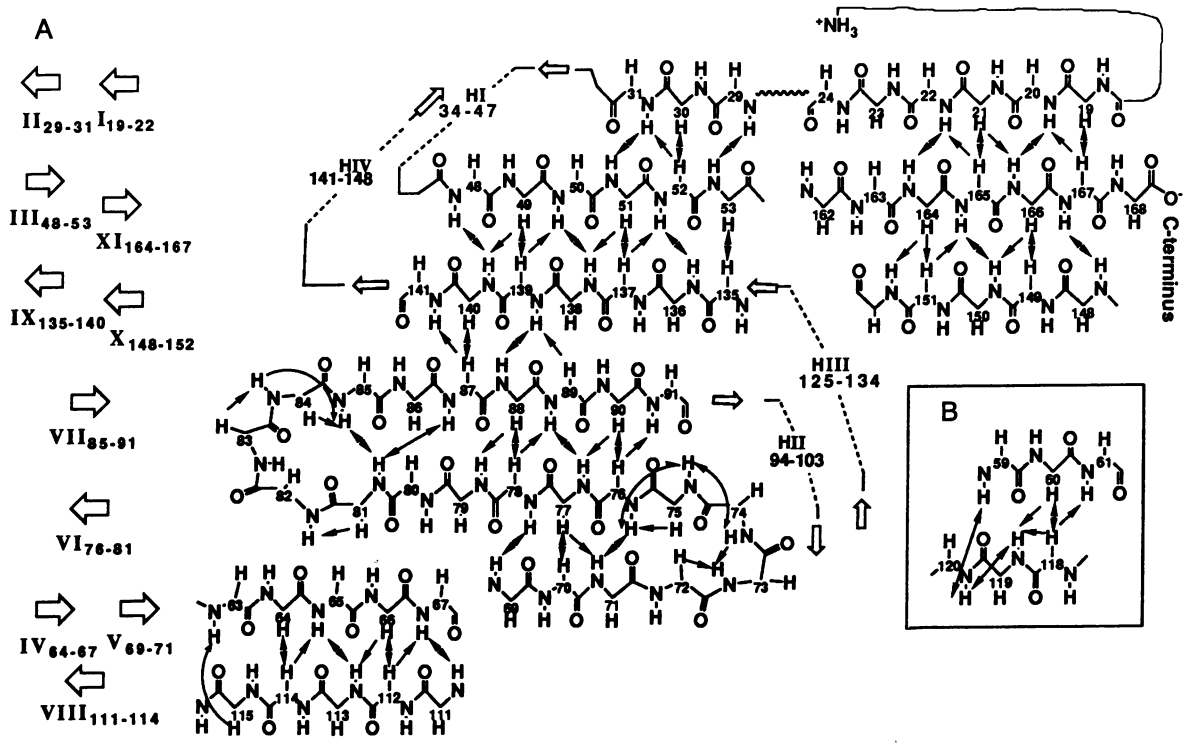

FIG. 3. (*A*) β-sheet structure of III^{Glc}. White arrows denote β-strands; black arrows represent long-range NOEs observed in 3D ^{15}N (d_{NN}, $d_{\alpha N}$) and ^{13}C ($d_{\alpha\alpha}$) NOESY-HMQC spectra. (*B*) Pattern of long-range NOEs seen between segments Met^{59}-Val^{63} and Val^{115}-Ile^{120}. Arrowheads represent observed direction of magnetization transfer.

the first 18 residues are highly disordered in solution. Our further observation, that deletion of the first seven residues does not affect the solution conformation of the structured portion of III^{Glc}, means that structural studies involving III^{Glc}_{fast} will be relevant to the solution structure of the intact protein.

We acknowledge Drs. A. Bax, M. Ikura, L. Kay, and D. Marion for providing pulse sequences and computer software needed to process the 3D data sets. We also thank R. Tschudin and R. Rendle for expert technical support. This work was supported by the AIDS Targeted Antiviral Program of the Office of the Director of the National Institutes of Health (to D.A.T.) and Grant GM38759 from the National Institutes of Health and Grant N00014-85-K-0072 from the Office of Naval Research (to S.R.) C.-Y.W. was supported by a Predoctoral Training Grant from the National Institutes of Health and is a W. R. Grace Predoctoral Fellow. This is contribution 1460 from the McCollum-Pratt Institute.

1. Meadow, N. D., Fox, D. K. & Roseman, S. (1990) *Annu. Rev. Biochem.* **59,** 497–542.
2. Postma, P. W. & Lengeler, J. (1985) *Microbiol. Rev.* **49,** 232–269.
3. Saier, M. H., Jr. (1989) *Microbiol. Rev.* **53,** 109–120.
4. Dörschug, M., Frank, R., Kalbitzer, H. R., Hengstenber, W. & Deutscher, J. (1984) *Eur. J. Biochem.* **144,** 113–119.
5. Presper, K. A., Wong, C.-Y., Lui, L., Meadow, N. D. & Roseman, S. (1989) *Proc. Natl. Acad. Sci. USA* **86,** 4052–4055.
6. Meadow, N. D., Coyle, P., Komoryia, A., Anfinsen, C. B. & Roseman, S. (1986) *J. Biol. Chem.* **261,** 13504–13509.
7. Jablonski, E. G., Brand, L. & Roseman, S. (1983) *J. Biol. Chem.* **258,** 9690–9699.
8. Kalbitzer, H. R., Deutscher, J., Hengstenberg, W. & Rösch, P. (1981) *Biochemistry* **20,** 6178–6185.
9. Kalbitzer, H. R., Muss, H. P., Engelmann, R., Kiltz, H. H., Stuber, K. & Hengstenberg, W. (1985) *Biochemistry* **24,** 4562–4569.
10. Kalbitzer, H. R., Hengstenberg, W., Rösch, P., Muss, H. P., Bernsmann, R. & Dörschung, M. (1982) *Biochemistry* **21,** 2879–2885.
11. Klevit, R. E., Drobny, G. & Waygood, E. B. (1986) *Biochemistry* **25,** 7760–7769.
12. Klevit, R. E. & Drobny, G. (1986) *Biochemistry* **25,** 7769–7773.
13. Klevit, R. E. & Waygood, E. B. (1986) *Biochemistry* **25,** 7774–7781.
14. El-Kabbani, A. L., Waygood, E. B. & Delbaere, L. T. J. (1987) *J. Biol. Chem.* **262,** 12926–12929.
15. Ikura, M., Kay, L. E. & Bax, A. (1990) *Biochemistry* **29,** 4659–4667.
16. Kay, L. E., Ikura, M., Tschudin, R. & Bax, A. (1990) *J. Magn. Reson.* **89,** 496–514.
17. Kay, L. E., Ikura, M. & Bax, A. (1990) *J. Am. Chem. Soc.* **112,** 888–889.
18. Bax, A., Clore, G. M., Driscoll, P. C., Gronenborn, A. M., Ikura, M. & Kay, L. E. (1990) *J. Magn. Reson.* **87,** 620–627.
19. Bax, A., Clore, G. M. & Gronenborn, A. M. (1990) *J. Magn. Reson.* **88,** 425–431.
20. Wüthrich, K. (1986) in *NMR of Proteins and Nucleic Acids* (Wiley, New York), pp. 162–174.
21. Kaptein, R., Boelens, R., Scheek, R. M. & van Gunsteren, W. F. (1988) *Biochemistry* **27,** 5389–5395.
22. Clore, G. M. & Gronenborn, A. M. (1989) *CRC Crit. Rev. Biochem. Biol.* **24,** 479–564.
23. Marion, D., Kay, L. E., Sparks, S. W., Torchia, D. A. & Bax, A. (1989) *J. Am. Chem. Soc.* **111,** 1515–1517.
24. Kay, L. E., Marion, D. & Bax, A. (1989) *J. Magn. Reson.* **84,** 72–84.
25. Ikura, M., Kay, L. E., Tschudin, R. & Bax, A. (1990) *J. Magn. Reson.* **86,** 204–209.
26. Driscoll, P. C., Gronenborn, A. M., Wingfield, P. T. & Clore, G. M. (1990) *Biochemistry* **29,** 4668–4682.
27. Studier, F. W. & Moffatt, B. A. (1986) *J. Mol. Biol.* **189,** 113–130.
28. Neidhardt, F. C., Block, P. L. & Smith, D. F. (1974) *J. Bacteriol.* **119,** 736–747.
29. Meadow, N. D. & Roseman, S. (1982) *J. Biol. Chem.* **257,** 14526–14537.
30. Marion, D., Ikura, M. & Bax, A. (1989) *J. Magn. Reson.* **84,** 425–430.
31. Live, D. H., Davis, D. G., Agosta, W. C. & Cowburn, D. (1984) *J. Am. Chem. Soc.* **106,** 1939–1941.
32. Barlow, D. J. & Thornton, J. M. (1988) *J. Mol. Biol.* **201,** 601–619.
33. Poolman, B., Royer, T. J., Mainzer, S. E. & Schmidt, B. F. (1989) *J. Bacteriol.* **171,** 244–253.